Journal of
Mechanics of
Materials and Structures

INFLUENCE OF THE ELASTIC PARAMETERS OF A FLUTTERING PLATE ON ITS POST-CRITICAL BEHAVIOR

Silvano Tizzi

Volume 2, Nº 5 May 2007

mathematical sciences publishers

JOURNAL OF MECHANICS OF MATERIALS AND STRUCTURES
Vol. 2, No. 5, 2007

INFLUENCE OF THE ELASTIC PARAMETERS OF A FLUTTERING PLATE ON ITS POST-CRITICAL BEHAVIOR

SILVANO TIZZI

A computational work to determine the post-critical flutter behavior of orthotropic and isotropic panels, according to the Von Karman's large deflection plate theory and quasisteady linearized aerodynamic theory, has been performed. Three different numerical schemes, based on Galerkin, Ritz and finite element method, have been employed for the integration over the panel surface, to reduce the mathematical problem to a system of differential equations in time. These can be integrated by appropriate algorithms to derive the vibrating plate behavior over time. Thus, it has been possible to determine a permanent solution in post-critical conditions. The paper focuses on the influence of the elastic parameters on the limit cycle solution of the vibrating plate under a high supersonic flow. Comparisons between the results obtained by panels with different elastic properties have been mandatory to characterize their effects on the post-critical flutter stationary solution. Particular attention has been given to the limit cycle amplitude, which is a fundamental parameter indicative of the fluttering panel resistance to a high supersonic airflow. Thus it has been possible to state an evaluation criterion of the hierarchic importance of the plate elastic parameters, based on their influence on the panel resistance to the post-critical flutter phenomenon. The reliability of our analysis can be guaranteed through the good agreement between the results of the three methods.

Notation

Roman letters

A_x, A_y	extensional rigidity parameters of the orthotropic plate
$A_r = A_{x,is} = A_{y,is}$	extensional rigidity parameter of the isotropic reference plate
a, b	rectangular plate dimensions
a_1, b_1	nondimensional parameters
a_{i_ψ}	coefficients of the nondimensional Airy function series expansion
$D_r = D_{x,is} = D_{y,is}$	flexural rigidity modulus of the reference isotropic plate
D_x, D_y, D_t	flexural and torsional rigidity moduli of the orthotropic plate
$E_{\Downarrow}$, $E_{\hookleftarrow}$	Young's moduli of the orthotropic plate along the fibers direction and the perpendicular one, respectively
E_x, E_y	Young's moduli of the orthotropic plate along the axes x and y, resp.
E_r	Young's modulus of the isotropic reference plate

Keywords: influence, elastic, parameters, plate, fluttering, post-critical, behavior.

$G_{xy} = G_{\Downarrow\hookleftarrow}$	in-plane shear rigidity modulus of the orthotropic plate
$G_r = G_{xy,is}$	in-plane shear rigidity modulus of the isotropic reference plate
h	plate thickness
k_{ij}	stiffness matrix elements
k^*_{ij}	elements of the linear structural-aerodynamic resultant forces matrix
L_a	nondimensional parameter L/a
L, L_w	in-plane and plate thickness reference lengths
M_{ach}	Mach number
m_{ij}	mass matrix elements
N	whole number of the Lagrangian d.o.f.
N_x, N_y, N_{xy}	in-plane membrane forces
t	time symbol
U_a	supersonic flow speed
U, V, W	nondimensional displacements along the axes x, y, z respectively
U_{i_U}, V_{i_V}, W_{i_W}	coefficients of the nondimensional displacements U, V, W series expansions
u, v, w	displacements along the axes x, y, z, respectively
x, y, z	plate reference system axes

Greek symbols

α_1, β_1, γ_1	flexural and torsional rigidity nondimensional parameters
β	nondimensional parameter equal to $\sqrt{M^2_{ach} - 1}$
γ	geometric nondimensional parameter
δ_{ij}	Kronecker's delta
ζ_{ij}	utilized matrix elements
ϑ	nondimensional parameter in the flutter vibration equation
λ	nondimensional dynamic pressure
ν_{xy}, ν_{yx}, $\nu_{\Downarrow\hookleftarrow}$, $\nu_{\hookleftarrow\Downarrow}$	Poisson's moduli of the orthotropic plate
ν_r	Poisson's modulus of the reference isotropic plate
ξ, η	nondimensional in-plane coordinates
τ	nondimensional time
Φ	Stress Airy function
φ_{i_ψ}	generic element in the nondimensional Airy function series expansion
$\chi_{i_U}\chi_{i_V}\chi_{i_W}$	generic elements of the displacements series expansions
ψ	nondimensional Airy function

Special symbols

∂	partial differentiation
$\mathfrak{d}^{(3)}_{ijk}$, $\mathfrak{d}^{(4)}_{ijkl}$, e_{ijkl}, h_{ijk}	tensor elements
$I^{(\,)}_{\ldots}$	generic integral
$[\boldsymbol{D}^{(4)}][\boldsymbol{E}][\boldsymbol{H}][\boldsymbol{T}][\boldsymbol{O}]$	utilized matrices
$[\boldsymbol{K}^{(op)}][\boldsymbol{M}^{(op)}]$	out-of-plane stiffness and mass matrices
$[\boldsymbol{K}^{(op)}]^*$	out-of-plane linear structural-aerodynamic forces matrix
$[\boldsymbol{Q}^{(op)}]$	out-of-plane Lagrangian degrees of freedom column vector
$[\boldsymbol{Q}^{(op,3)}]$	column vector containing the triple products of the out-of-plane Lagrangian degrees of freedom
$[\boldsymbol{W}]$	utilized column vector of the displacement W series expansions coefficients
$[\boldsymbol{W}^{(3)}]$	utilized column vector containing the triple products between coefficients of W series expansion
sin( ) cos( ) tan( )	trigonometric functions
$\mathcal{T}^{(\,)}$	nondimensional kinetic energy expression
$\mathcal{U}^{(\,)}_l \mathcal{U}^{(\,)}_m \mathcal{U}^{(\,)}_{nl}$	nondimensional strain energy expressions due to linear, mixed and nonlinear structural forces

Subscripts

i, j	subscripts with generic meaning
$\ldots, is; r$	subscripts referring to the isotropic plate
$i_U j_U k_U$, $i_V j_V k_V$	subscripts referring to U, V, W, respectively, in
$i_W j_W k_W$	the series expansions
j_{Wc2}, j_{Wc3}	contraction indices
l, m, nl	subscripts referring to the linear,mixed and nonlinear structural forces
$\Downarrow, \hookleftarrow$	subscripts referring to the fibers direction and its perpendicular one

Superscripts

(in)	in-plane situation
(op)	out-of-plane situation

Abbreviations and acronyms

d.o.f.	degree(s) of freedom
FEM	finite element method

1. Introduction

Post-critical flutter behavior of plates and shells exposed to a high supersonic flow has been a subject of major interest and wide research because of its outstanding importance in the aerospace field. In fact the life expectancy and survivability of fluttering panels on high supersonic aircraft depend substantially on their resistance to this phenomenon.

Von Karman's large deflection theory [Bolotin 1963], which takes into account the presence of nonlinear structural forces, together with the assumption of quasisteady first-order high supersonic theory [Bisplinghoff 1962], has been employed by most researchers in the field. The Galerkin method [Kantorowich and Krylov 1964; Mikhlin 1964] was utilized by Dowell [1966; 1967], and by Shiau and Lu [1992], and the Rayleigh-Ritz method [Reddy 1986] was used by Ketter [1967] and Eastep and McIntosh [1971] for the integration over the panel surface. By these methods it was possible to reduce the mathematical problem to a system of nonlinear ordinary differential equations in time, which was solved by numerical integration. Other researchers utilized the finite element method (FEM) [Kikuchi 1986; Reddy et al. 1988] to integrate over the plate or shell surface and to derive a system of ordinary differential equations in-time [Xue and Mei 1993; Dixon and Mei 1993; Zhou et al. 1994; Zhou et al. 1995; Zhou et al. 1996]. The Galerkin method was also used by [Abbas et al. 1993] to examine the problem of nonlinear aerothermoelasticity of panels in supersonic airflow.

A large amount of research was also conducted in the field of piezoelectric actuators to suppress large amplitude limit-cycle flutter [Zhou et al. 1995; Zhou et al. 1996]. Accurate dynamic analysis with actuators present was performed by the use of FEM. Furthermore, the effects of thermal loads were taken into account by some of the above mentioned authors [Xue and Mei 1993; Zhou et al. 1994; Zhou et al. 1995; Zhou et al. 1996; Abbas et al. 1993].

However, none of these authors has developed a particularized study on the influence of the elastic parameters of orthotropic and isotropic plates on the post-critical flutter behavior. One would expect that it would be of fundamental importance to know the role of each one of these parameters related to this phenomenon. For this reason, the main purpose of the present work focuses on their influence on the limit cycle stationary solution of the fluttering panel, whose amplitude determines its resistance to a high supersonic airflow.

First, the classical Galerkin method has been utilized, as in the Dowell's model. Then a Lagrangian functional expression has been formed to apply FEM and Ritz procedures [Tizzi 1994;1997; 2003a], and a system of ordinary differential equations in time has been obtained by the virtual work variational principle [Pars 1968], which has been integrated by appropriate algorithms.

Cases with different in-plane boundary conditions have been considered. For this reason two different models have been utilized with the Galerkin method. The first employs the Airy stress function to arrive at the classical von Karman's equations [Bolotin 1963]; the second one considers the in-plane displacements as unknown variables [Santini 1973].

A single model with the presence of a particular parameter can be employed instead, when FEM or Ritz procedures are utilized; this parameter takes into account the in-plane geometric boundary conditions in the in-plane clamped plate borders case [Tizzi 2003b].

The use of three different numerical schemes, giving very close results, can be helpful in guaranteeing the validity of the developed analysis.

The knowledge of the flutter behavior of a vibrating plate is useful also for multilayer composite laminates. In fact it is well known that the dynamic analysis of a nearly symmetric and balanced vibrating composite structure, angle-ply laminate $\pm\theta$ type, can be simulated by an equivalent orthotropic plate, with appropriate values for thickness and elastic parameters [Crivelli Visconti 1975; Tizzi 1999].

Consequently the present numerical analysis is useful also to characterize the resistance of a panel formed by a generic angle-ply composite laminate $\pm\theta$ with many component layers to air flowing at supersonic speed.

2. Mathematical formulations

Mathematical formulations have been developed for all three procedures treated in the paper.

A generic orthotropic plate, aligned with an x, y, z system of rectangular coordinates and exposed to a high supersonic airflow along the x axis, is considered and shown in Figure 1.

The Galerkin method has been utilized, then FEM and Ritz procedures have been used for the plate dynamic analysis.

The Einstein's summation convention for repeated indices has been adopted in all the forthcoming relations.

2.1. ***The Galerkin method.*** The out-of-plane vibration governing equation of a plate undergoing both extension and bending throughout its surface, combined with the transverse constitutive relations of orthotropic plates [Crivelli Visconti 1975], according to the Kirchhoff's hypothesis [Santini 1973], yields the second von Karman's governing equation of the flutter vibration, properly modified for an orthotropic

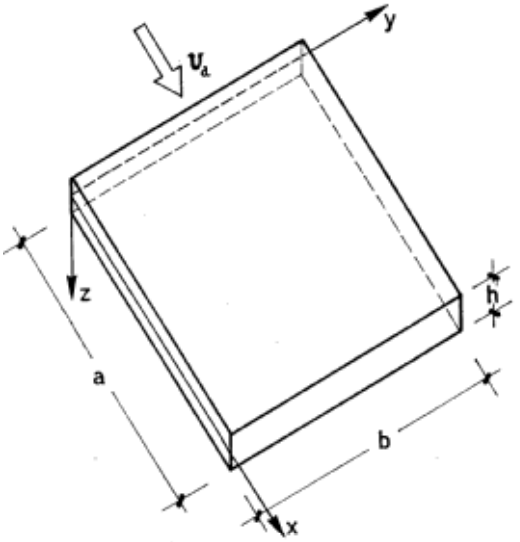

Figure 1. Plate exposed to an airflow at high supersonic speed.

plate:

$$D_x\frac{\partial^4 w}{\partial x^4}+2(\nu_{xy}D_y+2D_t)\frac{\partial^4 w}{\partial x^2\partial y^2}+D_y\frac{\partial^4 w}{\partial y^4}+p_z+\mu\frac{\partial^2 w}{\partial t^2}-N_x\frac{\partial^2 w}{\partial x^2}-2N_{xy}\frac{\partial^2 w}{\partial x\partial y}-N_y\frac{\partial^2 w}{\partial y^2}=0, \quad (1)$$

where $w(x, y, t)$ is the transverse displacement, N_x, N_y, N_{xy} are the membrane forces per unit length, and p_z is the aerodynamic loading pressure, which, within the framework of the quasisteady linearized "Piston Theory" of the high supersonic aerodynamics [Bisplinghoff 1962], is given by:

$$p_z=\frac{2q}{\beta}\left(\frac{\partial w}{\partial x}+\frac{1}{U_a}\frac{\beta^2-1}{\beta^2}\frac{\partial w}{\partial t}\right). \quad (2)$$

In Equation (2), $\beta^2=M_{ach}^2-1$, U_a is the high supersonic flow speed, and $q=\rho U_a^2/2$ is the air flowing dynamic pressure. Finally, the orthotropic plate flexural and torsional rigidity parameters are defined in the customary manner as:

$$D_x=\frac{E_x h^3}{1-\nu_{xy}\nu_{yx}}, \qquad D_y=\frac{E_y h^3}{1-\nu_{xy}\nu_{yx}}, \qquad D_t=G_{xy}\frac{h^3}{12}. \quad (3)$$

Since two different cases of the in-plane boundary conditions are considered, separate Galerkin procedures are utilized for the plate dynamic analysis.

Case 1. First, a simply supported plate for the out-of-plane behavior is considered, having the in-plane borders free—that is the membrane forces vanish on the limit edges:

$$\begin{aligned} &N_x=0 \qquad \text{and } N_{xy}=0 \quad \text{at } x=0, a\\ &N_y=0 \qquad \text{and } N_{xy}=0 \quad \text{at } y=0, a. \end{aligned} \quad (4)$$

The in-plane coordinates and the transverse displacement have been reformulated in nondimensional form:

$$\xi=\frac{x}{a}, \qquad \eta=\frac{y}{b}, \qquad W=\frac{w}{L_w}, \quad (5)$$

where L_w is the plate thickness reference length, and a, b are the rectangular plate dimensions.

The nondimensional transverse displacement is written in terms of a series expansion:

$$W(\xi,\eta,\tau)=W_{i_W}(\tau)\chi_{i_W}(\xi,\eta), \quad i_W=1,2,\ldots,N_W, \quad (6)$$

where each element $\chi_{i_W}(\xi,\eta)$ satisfies the boundary conditions of a simply supported plate, and can be defined as:

$$\chi_{i_W}(\xi,\eta)=\sin(i_{Wx}\pi\xi)\sin(i_{Wy}\pi\eta), \quad (7)$$

$$i_{Wx}=1,2,\ldots,N_{Wx}, \qquad i_{Wy}=1,2,\ldots,N_{Wy}, \qquad i_W=(i_{Wx}-1)N_{Wy}+i_{Wy}, \quad (8)$$

$$i_W=1,2,\ldots,N_W, \qquad N_W=N_{Wx}N_{Wy}. \quad (9)$$

Since the in-plane inertia is being neglected, in this particular case it is better to utilize the Airy stress function to describe the in-plane static behavior and hence to satisfy easily the natural boundary conditions in Equations (4).

This Airy function $\Phi(x, y, t)$ can be reformulated in nondimensional form:

$$\psi = \frac{\Phi}{E_r h L^2}, \tag{10}$$

where L is the in-plane reference length, E_r is the Young's modulus of the reference isotropic plate, and h is the plate thickness.

A series expansion for $\psi(\xi, \eta, \tau)$ in terms of function elements can be chosen:

$$\psi(\xi, \eta, \tau) = a_{i_\psi}(\tau)\varphi_{i_\psi}(\xi, \eta), \quad i_\psi = 1, 2, \ldots, N_\psi, \tag{11}$$

where the generic function element $\varphi_{i_\psi}(\xi, \eta)$ is equal to:

$$\begin{aligned} \varphi_{i_\psi}(\xi, \eta) &= \varphi_{i_{\psi x}}(\xi)\varphi_{i_{\psi y}}(\eta), \\ i_{\psi x} &= 1, 2, \ldots, N_{\psi x}, \\ i_{\psi y} &= 1, 2, \ldots, N_{\psi y}, \\ i_\psi &= (i_{\psi x} - 1)N_{\psi y} + i_{\psi y}, \\ i_\psi &= 1, 2, \ldots, N_\psi, \\ N_\psi &= N_{\psi x} N_{\psi y}, \end{aligned} \tag{12}$$

and further, $\varphi_{i_{\psi x}}(\xi)$, $\varphi_{i_{\psi y}}(\eta)$ are nearly orthonormal describing functions, which vanish with their first normal derivatives at the plate borders. Thus, for the membrane forces with dependence on the stress function, the natural boundary conditions in Equations (4) are satisfied. These are treated in the Appendix.

The in-plane compatibility relation [Santini 1973], by virtue of the in-plane kinematic and constitutive equations of an orthotropic plate [Crivelli Visconti 1975], together with the dependence of the membrane forces on the stress function, lead to the classical von Karman's first equation, properly modified for an orthotropic plate [Tizzi 2003b].

In view of the same membrane forces' dependence on the stress function, the flutter governing Equation (1), combined with the in-plane von Karman's first equation, through Galerkin operations becomes in nondimensional form:

$$\begin{aligned} &\ddot{W}_m + \sqrt{\lambda\vartheta}\,\dot{W}_m + i_{3W}^4 W_m + 4\lambda L_a I_{mj_W}^{(\chi\chi)} W_{j_W} \\ &\quad - \frac{4}{\pi^4} h L^2 a_1^2 b_1^2 \frac{\sqrt{E_x E_y}}{E_r} I_{mi_\psi i_W}^{(\chi\varphi\chi)} \zeta_{i_\psi j_W c2} W_{i_W} W_{j_W} W_{k_W} = 0 \quad m = 1, 2, \ldots, N_W, \end{aligned} \tag{13}$$

where

$$\begin{aligned} i_{3W}^4 &= \alpha_1^4 i_{Wx}^4 + \gamma_1^4 i_{Wx}^2 i_{Wy}^2 + \beta_1^4 i_{Wy}^4, \\ \dot{W}_{i_W} &= \frac{\partial W_{i_W}}{\partial \tau}, \\ \ddot{W}_{i_W} &= \frac{\partial^2 W_{i_W}}{\partial \tau^2}, \\ I_{mj_W}^{(\chi\chi)} &= \int_\Sigma \chi_m \frac{\partial \chi_{j_W}}{\partial \xi} d\Sigma, \end{aligned} \tag{14}$$

$$I^{(\chi\varphi\chi)}_{mi_\psi i_W} = \int_\Sigma \chi_m \left[\frac{\partial^2\varphi_{i_\psi}}{\partial\eta^2}\frac{\partial^2\chi_{i_W}}{\partial\xi^2} - 2\frac{\partial^2\varphi_{i_\psi}}{\partial\xi\,\partial\eta}\frac{\partial^2\chi_{i_W}}{\partial\xi\,\partial\eta} + \frac{\partial^2\varphi_{i_\psi}}{\partial\xi^2}\frac{\partial^2\chi_{i_W}}{\partial\eta^2} \right] d\Sigma. \tag{15}$$

Further, we have introduced in Equations (13) and (14) the following nondimensional parameters:

$$a_1 = \sqrt[4]{\frac{E_r}{E_y}}\frac{L}{a}, \qquad b_1 = \sqrt[4]{\frac{E_r}{E_x}}\frac{L}{b}, \qquad \gamma = \frac{L_w}{L}, \tag{16}$$

$$\alpha_1^4 = \frac{D_x L^4}{D_r a^4}, \qquad \beta_1^4 = \frac{D_y L^4}{D_r b^4}, \qquad \gamma_1^4 = \frac{2(\nu_{xy}D_y + 2D_t)}{D_r}\frac{L^4}{a^2b^2}, \qquad L_a = \frac{L}{a}, \tag{17}$$

$$\lambda = \frac{2qL^3}{\beta\pi^4 D_r}, \qquad \vartheta = \left(\frac{\beta^2-1}{\beta^2}\right)^2 \frac{2qL}{\beta\mu U_a^2}, \qquad \tau = \sqrt{\frac{D_r\pi^4}{\mu L^4}}\,t, \tag{18}$$

where E_r is the Young's modulus of the isotropic reference plate, and $D_r = E_r h^3/12(1-\nu_r^2)$ is the flexural rigidity modulus of the same fluttering reference plate.

Finally, the coefficients $\zeta_{i_\psi j_{Wc2}}$ in Equation (13) are matrix elements, connecting the coefficients a_{i_ψ} of the series in Equation (11), with the double product of the out-of-plane bending displacement series expansion coefficients in Equation (6):

$$a_{i_\psi} = \zeta_{i_\psi j_{Wc2}} W_{j_W} W_{k_W}. \tag{19}$$

In Equation (19) j_{Wc2} is the contraction of the two indices j_W and k_W.

Detailed explanations of the analytical developments which, starting from the flutter Equation (1) and the in-plane static equilibrium von Karman's relation, allow us to derive, through Galerkin operations, the governing Equation (13) and the relation (19), are shown in [Tizzi 2003b]. These developments are very similar to those in the analytical studies carried out by other authors [Dowell 1966; Dowell 1967; Shiau and Lu 1992; Abbas et al. 1993].

Equation (13) can be transformed into its equivalent matrix form:

$$[\ddot{\boldsymbol{W}}] + \sqrt{\lambda\vartheta}[\dot{\boldsymbol{W}}] + i_3^4[\boldsymbol{W}] + [\boldsymbol{H}][\boldsymbol{W}] - [\boldsymbol{O}][\boldsymbol{W}^{(3)}] = 0, \tag{20}$$

where $[\boldsymbol{W}]$ is the column vector having dimensions N_W, whose elements are the series expansions coefficients of the transverse displacement in Equation (6); $[\boldsymbol{W}^{(3)}]$ is the column vector with dimensions N_W^3, whose elements are the triple products of the same coefficients $p^{(3)}_{j_{Wc3}} = W_{i_W} p^{(2)}_{j_{Wc2}} = W_{i_W} W_{j_W} W_{k_W}$ (j_{Wc3} is the contraction of the three indices i_W, j_W, k_W or i_W, j_{Wc2}); $[\boldsymbol{H}]$ and $[\boldsymbol{O}]$ are matrices, having dimensions $N_W \times N_W$ and $N_W \times N_W^3$, respectively, whose elements are:

$$h_{mj_W} = 4\lambda L_a I^{(\chi\chi)}_{mj_W}, \qquad o_{mj_{Wc3}} = 4hL^2 a_1^2 b_1^2 \frac{\sqrt{E_x E_y}}{E_r} I^{(\chi\varphi\chi)}_{mi_\psi i_W}\zeta_{i_\psi j_{Wc2}}. \tag{21}$$

In the second of Equations (21) the summation convention for the repeated index i_ψ has been utilized.

Thus, a reduced system of nonlinear differential equations is derived, with a single independent variable W. For the integration in time, an algorithm based on the Kutta-Merson procedure is utilized, with variable control of the step integration [Merson 1957; Lambert 1991].

Case 2. We then analyze a second case of a plate, likewise simply supported at the borders for the transverse behavior but clamped at the four edges for the in-plane displacements. In place of Equations (4) there are the following boundary conditions for in-plane displacements:

$$u = 0 \qquad \text{and} \qquad v = 0 \qquad \text{at} \qquad x = 0, a \qquad \text{and} \qquad y = 0, b. \tag{22}$$

In this case it is not convenient to use the Airy function, but to set-up the in-plane governing equations by means of the membrane displacements functions over the mid-plane panel surface.

Like the transverse displacement $W = w/L_w$, as in the third of Equations (5), the in-plane displacements u, v have also been reformulated in nondimensional form:

$$U = \frac{u}{a}\frac{1}{\gamma_a^2}, \qquad V = \frac{v}{b}\frac{1}{\gamma_b^2}. \tag{23}$$

Notice that the order of magnitude of the in-plane displacements u, v is the same as that of w^2; thus the same order of magnitude corresponds to U, V, W.

Appropriate series expansions have been chosen for the nondimensional in-plane displacements:

$$U = U_{i_U}(\tau)\chi_{i_U}(\xi, \eta), \qquad V = V_{i_V}(\tau)\chi_{i_V}(\xi, \eta), \quad i_U, i_V = 1, 2, \ldots, N_U, N_V, \tag{24}$$

where each function element of the series is defined as

$$\begin{aligned} \chi_{i_U}(\xi, \eta) &= \sin(i_{Ux}\pi\xi)\sin(i_{Uy}\pi\eta) \\ \chi_{i_V}(\xi, \eta) &= \sin(i_{Vx}\pi\xi)\sin(i_{Vy}\pi\eta) \end{aligned} \tag{25}$$

$$\begin{aligned} &i_{Ux}, i_{Vx} = 1, 2, \ldots, N_{Ux}, N_{Vx}, \\ &i_{Uy}, i_{Vy} = 1, 2, \ldots, N_{Uy}, N_{Vy}, \\ &\quad i_U, i_V = (i_{Ux}, i_{Vx} - 1)N_{Uy}, N_{Vy} + i_{Uy}, i_{Vy}, \\ &\quad i_U, i_V = 1, 2, \ldots, N_U, N_V, \\ &N_U, N_V = N_{Ux}, N_{Vx} \times N_{Uy}, N_{Vy} \end{aligned} \tag{26}$$

which satisfy the boundary conditions in Equations (22).

Also, in this case, the in-plane inertia effects are being neglected. The static equilibrium equations along the x and y axes, for the in-plane kinematic and constitutive relationships of an orthotropic plate, expressed in terms of the membrane displacements [Santini 1973; Crivelli Visconti 1975], can be determined [Tizzi 2003b].

The von Karman's flutter vibration Equation (1), in view of the same in-plane kinematic and constitutive relations of an orthotropic plate, combined with the two in-plane static equilibrium equations, through Galerkin operations becomes

$$\ddot{W}_m + \sqrt{\lambda\vartheta}\,\dot{W}_m + i_{3W}^4 W_m + 4\lambda L_a I_{m j_W}^{(\chi\chi)} W_{j_W} + t_{m j_W c3} W_{i_W} W_{j_W} W_{k_W} = 0, \quad m = 1, 2, \ldots, N_W, \tag{27}$$

where the time derivatives, along with the parameter i_{3W}^4 and the integral $I_{m j_W}^{(\chi\chi)}$, have been previously defined in Equations (14), and the meaning of the nondimensional parameters λ and ϑ is explained in Equations (18).

Furthermore $t_{mj_{Wc3}}$ are matrix elements, where j_{Wc3} is the contraction of the three indices i_W, j_W, k_W, as stated after Equation (20).

Detailed explanations of the analytical developments, which, starting from the flutter Equation (1), and combined with the two in-plane static equilibrium relations, allow us to find the governing Equation (27) through Galerkin operations, are given in [Tizzi 2003b].

Introducing the matrix $[\boldsymbol{T}]$, having elements $t_{mj_{Wc3}}$ and dimensions $N_W \times N_W^3$, allows Equation (27) to take its equivalent matrix form:

$$[\ddot{\boldsymbol{W}}] + \sqrt{\lambda\vartheta}[\dot{\boldsymbol{W}}] + i_{3W}^4[\boldsymbol{W}] + [\boldsymbol{H}][\boldsymbol{W}] - [\boldsymbol{T}][\boldsymbol{W}^{(3)}] = 0, \tag{28}$$

where the same column vector $[\boldsymbol{W}^{(3)}]$, previously defined after Equation (20), and the same matrix $[\boldsymbol{H}]$, whose elements have been defined in the first of Equations (21), are utilized. The same algorithm, applying the Kutta-Merson procedure with variable step control for the integration in time, is utilized, as it is for the differential relations system in Equation (20).

2.2. ***Ritz and FEM procedures.*** Procedures built both on the Rayleigh-Ritz method and on FEM [Tizzi 1994; 1997; 2003a] have been employed to extract the requested results. These arise from differential operations on an energetic functional, whose stationary conditions lead to the dynamic governing equations. Since with FEM or Ritz method one is not obliged to satisfy the natural boundary conditions in the free in-plane edges case, as in Equation (4), the same model can be utilized for the two cases with different in-plane conditions at the panel borders. It is only sufficient to introduce a parameter which takes into account the geometric in-plane boundary conditions in the in-plane clamped plate edges case.

The strain energy expression, due to the in-plane and transverse linear structural forces only, can be stated as:

$$U_l^{(in)} = \tfrac{1}{2}k_{ij}^{(in)}q_i^{(in)}q_j^{(in)}, \qquad U_l^{(op)} = \tfrac{1}{2}k_{ij}^{(op)}q_i^{(op)}q_j^{(op)}, \tag{29}$$

where

(1) $k_{ij}^{(in)}$ and $k_{ij}^{(op)}$ are the in-plane and out-of-plane stiffness matrix elements of the orthotropic plate, respectively, which have been previously evaluated both for Ritz and for FEM procedure,

(2) $q_i^{(in)}$, $q_j^{(in)}$ and $q_i^{(op)}$, $q_j^{(op)}$ are the in-plane and out-of-plane transverse degrees of freedom (d.o.f.), respectively, of both methods.

In the Ritz procedure, these stand for the coefficients of the polynomial series expansions of the in-plane and transverse displacements, respectively, as in Equations (24) and (6), whereas in the FEM, these correspond to the same displacements and their first order derivatives in the in-plane coordinates on the grid points of the chosen mesh [Tizzi 2003b].

Also the contribution of the mixed and nonlinear structural forces to the in-plane strain energy can be evaluated and expressed as:

$$\mathcal{U}_m^{(in)} = \tfrac{1}{2}\mathfrak{d}_{ijk}^{(3)}q_i^{(in)}q_j^{(op)}q_k^{(op)}, \qquad \mathcal{U}_{nl}^{(in)} = \tfrac{1}{2}\mathfrak{d}_{ijkl}^{(4)}q_i^{(op)}q_j^{(op)}q_k^{(op)}q_l^{(op)}, \tag{30}$$

where $\mathfrak{d}_{ijk}^{(3)}$ and $\mathfrak{d}_{ijkl}^{(4)}$ are tensor elements, previously determined in the Ritz and FEM procedures [Tizzi 2003b].

The in-plane and transverse kinetic energy expressions can be stated in the classical form:

$$\mathcal{T}^{(in)} = \tfrac{1}{2} m_{ij}^{(in)} \dot{q}_i^{(in)} \dot{q}_j^{(in)}, \qquad \mathcal{T}^{(op)} = \tfrac{1}{2} m_{ij}^{(op)} \dot{q}_i^{(op)} \dot{q}_j^{(op)}, \tag{31}$$

where $\dot{q}_i, \dot{q}_j = \partial[q_i, q_j]/\partial\tau$, and $m_{ij}^{(in)}$, $m_{ij}^{(op)}$ are the in-plane and out-of-plane mass matrix elements, respectively. Also these have been previously evaluated for a fluttering orthotropic plate using both procedures [Tizzi 2003b]. Since the in-plane inertia effects have been neglected, the component $\mathcal{T}^{(in)}$ of the kinetic energy is not considered, and consequently only the elements $m_{ij}^{(op)}$ of the mass matrix are taken into account.

The Lagrangian $\mathcal{L}_a$ functional can be introduced:

$$\mathcal{L}_a = \mathcal{T}^{(op)} - \mathcal{U}_l^{(in)} - \mathcal{U}_l^{(op)} - \mathcal{U}_m^{(in)} - \mathcal{U}_{nl}^{(in)}. \tag{32}$$

The differential principle of virtual work, applied to the $i-th$ in-plane (in) or out-of-plane (op) d.o.f, leads to the classical Lagrange equation [Pars 1968]:

$$\frac{d(\partial \mathcal{L}_a / \partial \dot{q}_i^{(in,op)})}{d\tau} - \frac{\partial \mathcal{L}_a}{\partial q_i^{(in,op)}} = 0. \tag{33}$$

This gives the in-plane or out-of-plane governing equations, depending on whether the generic degree of freedom refers to in-plane $q_i^{(in)}$ or the out-of-plane $q_i^{(op)}$ behavior.

Combining the two equations, and taking into account the aerodynamic generalized force presence in the out-of-plane governing equation, leads to:

$$m_{ij}^{(op)} \ddot{q}_j^{(op)} + f_{ij}^{(t)} \dot{q}_j^{(op)} + (k_{ij}^{(op)})^* q_j^{(op)} + e_{iklm} q_k^{(op)} q_l^{(op)} q_m^{(op)} + 2\mathfrak{d}_{ijkl}^{(4)} q_j^{(op)} q_k^{(op)} q_l^{(op)} = 0, \tag{34}$$

where the elements:

$$(k_{ij}^{(op)})^* = k_{ij}^{(op)} + f_{ij}^{(x)} \tag{35}$$

collect both the linear out-of-plane structural and aerodynamic coupling forces [Tizzi 1994]. Furthermore, the coefficients $f_{ij}^{(x)}$ and $f_{ij}^{(t)}$ appear in the expressions of the two components of the generalized aerodynamic force:

$$F_i^{(a)} = F_i^{(a,x)} + F_i^{(a,t)} \qquad F_i^{(a,x)} = f_{ij}^{(x)} q_j^{(op)}, \qquad F_i^{(a,t)} = f_{ij}^{(t)} \dot{q}_j^{(op)}. \tag{36}$$

The component $F_i^{(a,x)}$, containing the transverse displacement derivative in the x coordinate, is responsible for the coupling between different natural vibrating modes, while the damping component $F_i^{(a,t)}$, contains the transverse displacement time derivative, according to the linearized Piston Theory.

Detailed explanations of the way in which Equation (34) is derived, starting from the two in-plane and out-of-plane governing equations, are given in [Tizzi 2003b], where the meaning of the tensor elements e_{iklm} is sufficiently illustrated. The other tensor elements $\mathfrak{d}_{ijk}^{(4)}$ are the same as in the second of Equations (30).

The out-of-plane mass matrix $[\boldsymbol{M}^{(op)}]$, having elements $m_{ij}^{(op)}$, and the linear structural-aerodynamic forces matrix $[\boldsymbol{K}^{(op)}]^*$, having elements $(k_{ij}^{(op)})^*$, are introduced, together with the nonlinear structural forces matrices $[\boldsymbol{E}]$ and $[\boldsymbol{D}^{(4)}]$, having tensor elements $e_{ij_{c3}}$ and $\mathfrak{d}_{ij_{c3}}^{(4)}$, respectively ($j_{c3}$ is the contraction

index of the three indices k, l, m or j, k, l). The column vectors $[\boldsymbol{Q}^{(op)}]$, having elements the out-of-plane d.o.f. $q_i^{(op)}$, and $[\boldsymbol{Q}^{(op,3)}]$, containing the triple products

$$p_{j_{c3}}^{(3)} = q_k^{(op)} q_l^{(op)} q_m^{(op)} \quad \text{or} \quad p_{j_{c3}}^{(3)} = q_j^{(op)} q_k^{(op)} q_l^{(op)}$$

are also introduced. The elements $f_{ij}^{(t)}$ of the aerodynamic damping forces are proportional to the out-of-plane mass matrix elements $m_{ij}^{(op)}$ [Tizzi 2003a; 2003b]:

$$f_{ij}^{(t)} = \gamma_d m_{ij}^{(op)}. \tag{37}$$

Hence, the matrix having elements $f_{ij}^{(t)}$ would be coincident with the out-of-plane mass matrix $[\boldsymbol{M}^{(op)}]$, but for a coefficient γ_d, both for Ritz and for FEM methods.

This allows Equation (34) to take its equivalent matrix form:

$$[\ddot{\boldsymbol{Q}}^{(op)}] + \gamma_d [\dot{\boldsymbol{Q}}^{(op)}] + [\boldsymbol{M}^{(op)}]^{-1} [\boldsymbol{K}^{(op)}]^* [\boldsymbol{Q}^{(op)}] + [\boldsymbol{M}^{(op)}]^{-1} \{[\boldsymbol{E}] + 2[\boldsymbol{D}^{(4)}]\} [\boldsymbol{Q}^{(op,3)}] = 0. \tag{38}$$

A nonlinear equations system is obtained, similar to the one in Equation (28), which likewise can be integrated by an algorithm utilizing the Kutta-Merson procedure with variable integration step.

3. Applications and results

The introduced numerical approaches have been applied to different cases of orthotropic and isotropic plates. In all the considered cases the following geometric characteristics of the rectangular plates are supposed:

$$L = a = b = 100 L_w = 100 h, \tag{39}$$

and concerning the nondimensional parameter ϑ in the second of Equations (18), it has been assumed that

$$\vartheta = 0.1. \tag{40}$$

The in-plane and out-of-plane boundary conditions of the reference vibrating isotropic plate are the same as those for the fluttering orthotropic plate in every considered case.

The amplitude W_A of the flutter vibration displacement is evaluated in the point with maximum value of the transverse deflection $w(x, y, t)$, which verifies at about 3/4 of the central side parallel to the airflow direction, starting from the leading edge. This is a parameter of great importance; in fact the smaller this amplitude is, the higher is the resistance of the fluttering plate under the effects of air flowing at supersonic speed.

In the first two cases an orthotropic plate of composite u.d. materials, made of glass fibers and epossidic resin, is used, having the following elastic properties [Crivelli Visconti 1975]:

$$E_{\Downarrow} = 45\,\text{GPa}, \quad E_{\hookleftarrow} = 14\,\text{GPa}, \quad G_{\Downarrow\hookleftarrow} = 6\,\text{GPa}, \quad \nu_{\Downarrow\hookleftarrow} = 0.24, \quad \nu_{\hookleftarrow\Downarrow} = 0.0746, \tag{41}$$

where $E_{\Downarrow}$ is the Young's modulus along the fibers direction, $E_{\hookleftarrow}$ is the Young's modulus along the perpendicular direction, $G_{\Downarrow\hookleftarrow}$ is the shear rigidity modulus between the two directions, and $\nu_{\Downarrow\hookleftarrow}$, $\nu_{\hookleftarrow\Downarrow}$ denote the two Poisson's moduli. These are equal to ν_{xy}, ν_{yx} if the fibers are oriented in the airflow direction, and ν_{yx}, ν_{xy} if the fibers are oriented in the perpendicular direction.

λ	1.47	2.0	3.78	4.0	5.21	6.0	8.0	10.0	12.0	14.0	16.0
$E_x < E_y = E_r$	0	2.53		8.56		11.57	13.24	14.42	15.16	15.47	15.57
$E_x = E_r > E_y$			0	0.43		3.15	4.63	5.66	6.53	7.26	7.79
isotropic					0	0.70	2.01	2.84	3.47	4.0	4.42

Table 1. Values of the post-critical limit cycle amplitude W_A versus the nondimensional dynamic pressure λ in the first case.

In the first case considered, for a significant comparison of the results obtained, a reference isotropic plate is utilized having Young's modulus E_r equal to the higher of the two of the orthotropic plate and a Poisson's modulus $\nu_r = 0.3$. The plate is simply supported for the out-of-plane flutter dynamics, but with free in-plane boundary conditions, as in Equation (4).

The behavior of the limit cycle highest amplitude W_A versus the nondimensional dynamic pressure λ in Figure 2, corresponds to the post-critical dynamics of the orthotropic plate with the fibers oriented in the perpendicular direction to the airflow. In this subcase the Young's modulus along the x axis (direction of the airflow) is lower than the corresponding one along the perpendicular axis y ($E_x < E_y = E_r$), because $E_x = E_{\hookleftarrow}$ and $E_y = E_{\Downarrow}$. The lowest amplitude graph corresponds to the flutter of the reference isotropic vibrating plate. The middle amplitude curve of the flutter oscillations corresponds to the limit cycle of the orthotropic plate, with the fibers oriented in the airflow direction. In this second subcase, the Young's modulus along the x axis is higher than the corresponding one along the perpendicular direction ($E_x = E_r > E_y$), because $E_x = E_{\Downarrow}$ and $E_y = E_{\hookleftarrow}$.

The data points, which in Figure 2 appear as dots, are summarized in Table 1.

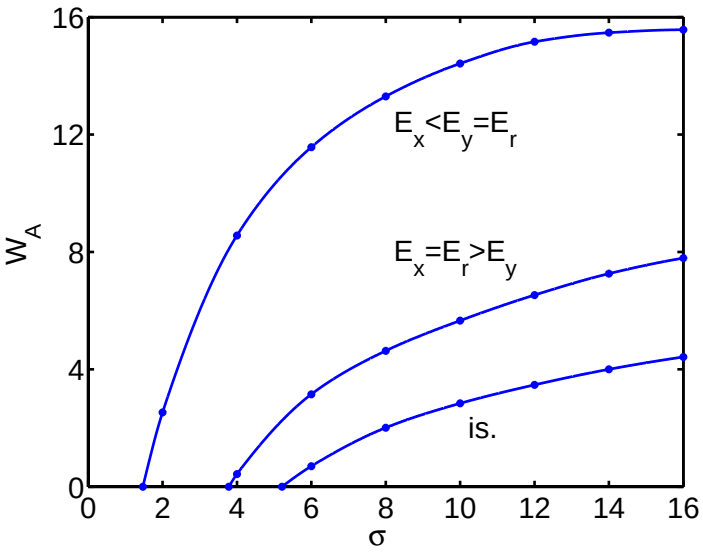

Figure 2. Behavior of the post-critical limit cycle amplitude W_A versus the nondimensional dynamic pressure λ in the first considered case.

λ	4.26	4.89	6.0	12.0	12.31	18.0	24.0	30.0	36.0	42.0	48.0
$E_x = E_r < E_y$	0		2.28	7.79		11.05	12.98	14.00	14.63	15.15	15.47
isotropic		0	0.8	3.68		5.26	6.42	7.16	7.79	8.30	8.84
$E_x > E_y = E_r$					0	2.95	4.57	5.47	6.31	7.05	7.68

Table 2. Values of the post-critical limit cycle amplitude W_A versus the nondimensional dynamic pressure λ in the second case.

In the second case, the same vibrating orthotropic plate of the previous case is considered, with the same in-plane and out-of-plane boundary conditions, but the Young's modulus E_r of the reference isotropic plate is equal to the smaller of the two ones of the orthotropic plate. Since the dynamic pressure has been reformulated in nondimensional form by dividing by the flexural rigidity modulus D_r of the isotropic plate (see the first of Equations (18)), which is lower than the corresponding one in the previous case, higher values of λ, compared to those in Figure 2, are noticed (see Figure 3).

In the same Figure 3, the curve of the highest amplitude behavior versus λ corresponds to the orthotropic plate with the fiber direction perpendicular to that of the airflow ($E_x = E_r < E_y$), whereas the lowest flutter amplitude chart corresponds to the fiber orientation in the airflow direction ($E_x > E_y = E_r$). The graphic curve of the limit cycle amplitude behavior versus λ of the isotropic plate, with lower Young's and equal Poisson's modulus with respect to the same parameter values of the previous case, is located between the two ones of the orthotropic plate.

The data points, which in Figure 3 appear as dots, are written in Table 2.

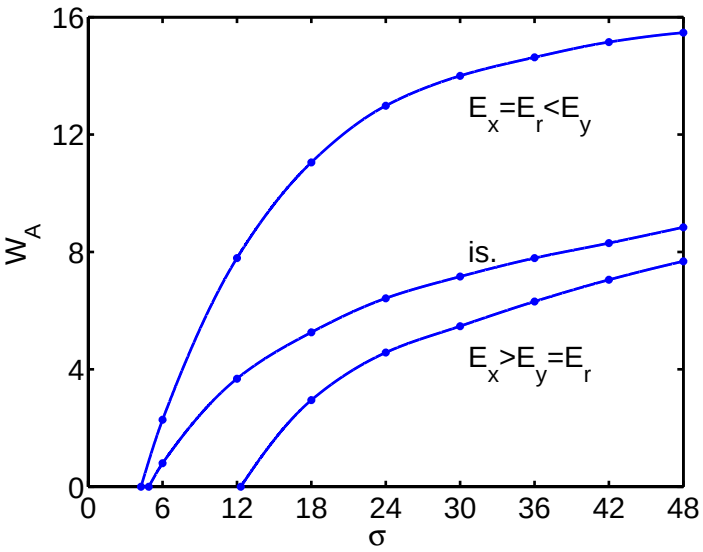

Figure 3. Behavior of the post-critical limit cycle amplitude W_A versus the nondimensional dynamic pressure λ in the second considered case.

λ	0.94	2.0	3.43	4.0	5.37	6.0	8.0	10.0	12.0	14.0	16.0
$E_x < E_y = E_r$	0	3.59		10.0		15.0	18.91	21.87	24.06	25.31	26.25
$E_x = E_r > E_y$			0	2.19		6.65	9.06	11.25	12.97	14.69	16.25
isotropic					0	0.94	2.45	2.90	3.20	3.62	3.91

Table 3. Values of the post-critical limit cycle amplitude W_A versus the nondimensional dynamic pressure λ, in the third case.

The third case refers to an orthotropic plate of composite u.d. materials, made of carbon fibers and epoxy resin type C3, and having the following elastic parameters [Crivelli Visconti 1975]:

$$E_{\Downarrow} = 107\,\text{GPa}, \quad E_{\hookleftarrow} = 7\,\text{GPa}, \quad G_{\Downarrow\hookleftarrow} = 6\,\text{GPa}, \quad \nu_{\Downarrow\hookleftarrow} = 0.24, \quad \nu_{\hookleftarrow\Downarrow} = 0.0157. \tag{42}$$

The in-plane and out-of-plane boundary conditions are the same as in the previous cases. In Figure 4 the curve of the highest amplitude behavior versus λ corresponds to the orthotropic plate with the fibers lined up in the perpendicular direction to the airflow, i.e. $E_x = E_{\hookleftarrow}$ and $E_y = E_{\Downarrow}$ ($E_x < E_y = E_r$). The lowest amplitude graph corresponds to the flutter limit cycle of the isotropic plate, with the Young's modulus equal to the higher of the two Young's moduli of the orthotropic plate, and likewise $\nu_r = 0.3$. The graphic curve located between the two previous ones corresponds to the orthotropic plate with the fibers aligned along the airflow direction, i.e. $E_x = E_{\Downarrow}$ and $E_y = E_{\hookleftarrow}$ ($E_x = E_r > E_y$).

The data points, which in Figure 4 appear as dots, are shown in Table 3.

The fourth case refers to the same orthotropic plate of the previous case, but with the Young's modulus E_r of the isotropic reference plate equal to the lower of E_x and E_y.

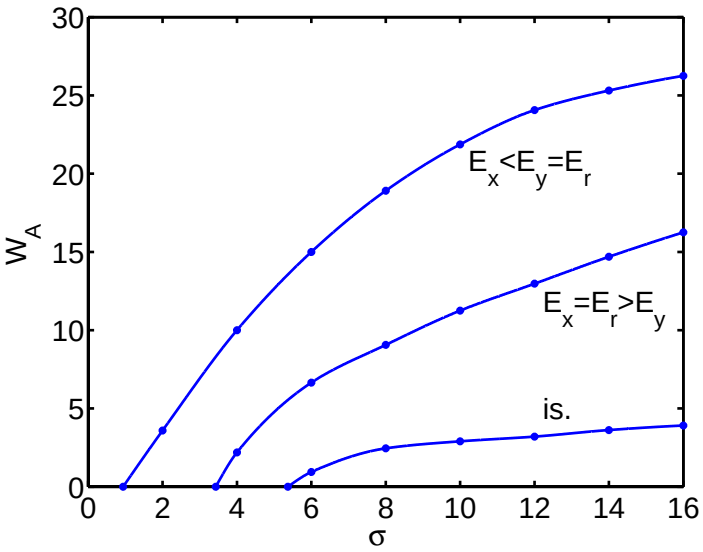

Figure 4. Behavior of the post-critical limit cycle amplitude W_A versus the nondimensional dynamic pressure λ in the third case considered.

λ	14.06	20.62	30.0	52.45	60.0	90.0	120.0	150.0	180.0	210.0	240.0
$E_x = E_r < E_y$	0		3.58		9.98	14.96	18.85	21.78	23.92	25.15	26.06
isotropic		0	2.19		6.43	9.52	11.76	13.34	14.78	15.95	17.03
$E_x > E_y = E_r$				0	2.18	6.63	9.02	11.17	12.82	14.45	16.00

Table 4. Values of the post-critical limit cycle amplitude W_A versus the nondimensional dynamic pressure λ, in the fourth case.

Figure 5 shows:

(1) the highest amplitude graphic line, corresponding to the orthotropic plate with the fibers aligned along the perpendicular direction to the airflow ($E_x = E_r < E_y$);

(2) the middle amplitude graph, corresponding to the isotropic reference plate;

(3) the lowest amplitude chart line, corresponding to the orthotropic plate with the fibers aligned in the airflow direction ($E_x > E_y = E_r$), as in the second case.

The reason for which the values of λ in Figure 5 differ from those in Figure 4, though they refer to the same orthotropic plate, is the same as that explained above for the second case.

The data points, which in Figure 5 appear as dots, are summarized in Table 4.

The orthotropic fluttering plate described in the two last cases is the same as that of the first two cases, but there are different in-plane boundary conditions, with rectangular edges clamped for the in-plane displacements, whereas the same simply supported plate boundary conditions are supposed for the out-of-plane flutter behavior.

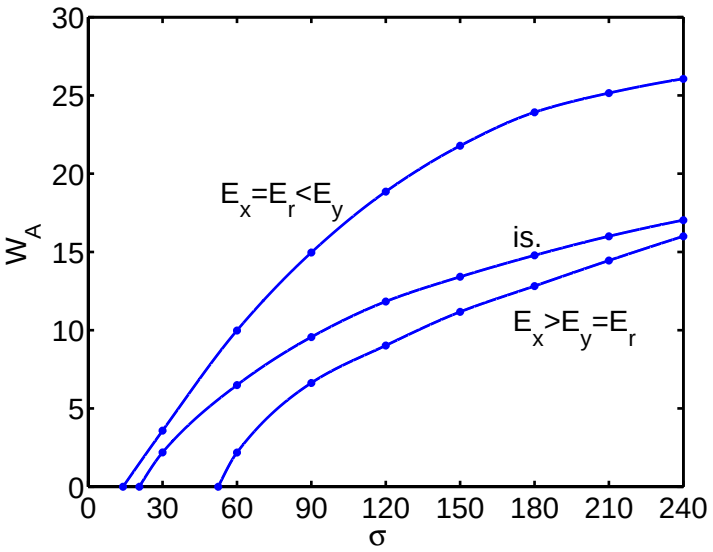

Figure 5. Behavior of the post-critical limit cycle amplitude W_A versus the nondimensional dynamic pressure λ in the fourth case considered.

λ	1.69	2.0	4.0	5.56	6.0	8.0	10.0	12.0	14.0	16.0
$E_x < E_y = E_r$	0	0.37	2.16		3.53	4.49	5.12	5.53	5.75	5.875
$E_x = E_r > E_y$			0		0.56	0.79	0.92	1.00	1.07	1.13
isotropic				0	0.18	0.62	0.75	0.81	0.875	0.91

Table 5. Values of the post-critical limit cycle amplitude W_A versus the nondimensional dynamic pressure λ, in the fifth case.

The fifth case refers to the isotropic plate with the Young's modulus E_r equal to the higher of E_x and E_y, as in the first and third cases. Figure 6 exhibits the behavior versus λ of the limit cycle amplitude of the orthotropic plate both for $E_x < E_y = E_r$ and for $E_x = E_r > E_y$, respectively, and also of the isotropic plate with the smallest limit cycle amplitude values, as in Figures 2 and 4.

The data points, which in Figure 6 appear as dots, are written in Table 5.

Figure 7 shows the behavior versus λ of the flutter modal amplitude of the same orthotropic plate described in the fifth case, but with the Young's modulus of the reference isotropic plate equal to the lower of E_x and E_y, as in the second and fourth cases. In this last sixth case, the graph of the lowest amplitude behavior versus λ corresponds to the orthotropic plate with fibers aligned along the airflow direction ($E_x > E_y = E_r$). The highest amplitude curve corresponds to the orthotropic plate with the fibers aligned along the perpendicular direction ($E_x = E_r < E_y$). The chart line of the isotropic plate is located between the two previous ones, as in Figure 3 and Figure 5. Also in this last case, as in the second and fourth cases, higher values of λ can be pointed out with respect to the previous case for the same above illustrated reason.

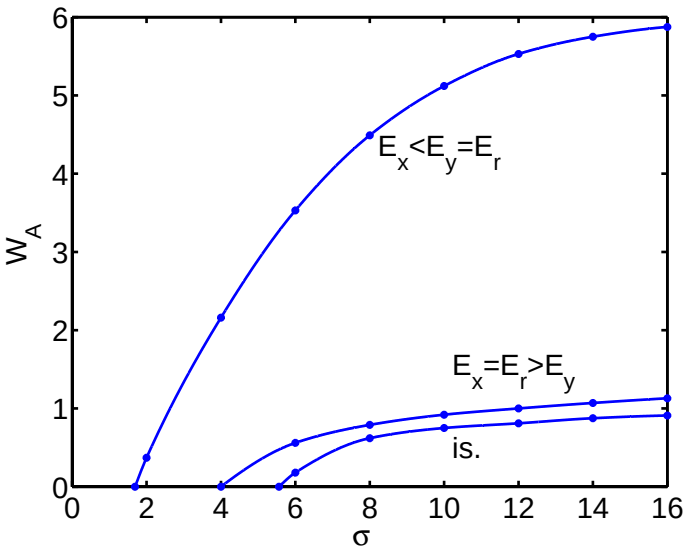

Figure 6. Behavior of the post-critical limit cycle amplitude W_A versus the nondimensional dynamic pressure λ in the fifth considered case.

λ	4.89	5.68	6.0	7.0	9.0	12.0	12.63	18.0	24.0	30.0	36.0	42.0	48.0
$E_x = E_r < E_y$	0.		0.33			2.05		3.37	4.32	5.0	5.45	5.71	5.87
isotropic		0.	0.16	0.42	0.65	0.79		0.97	1.08	1.18	1.26	1.30	1.33
$E_x > E_y = E_r$							0.	0.53	0.78	0.86	0.94	1.00	1.03

Table 6. Values of the post-critical limit cycle amplitude W_A versus the nondimensional dynamic pressure λ, in the sixth case.

The data points, which in Figure 7 appear as dots, are shown in Table 6.

To compare the amplitude values for limit cycles thus obtained with those found by other authors who use similar numerical schemes to find post-critical flutter solutions, one must take into account that our expression for the nondimensional dynamic pressure (first equation in (18)) differs from its nearest equivalent in those authors' works by the presence of π^4 in the denominator. Thus their values should be divided by approximately 100 ($\sim \pi^4$) for comparison with ours. With this precaution, we see that our limit cycles amplitudes are indeed comparable to those in the literature [Eastep and McIntosh 1971; Shiau and Lu 1992; Xue and Mei 1993].

Table 7 shows the frequencies values versus the nondimensional dynamic pressure, in the last considered case. Similar dependence verifies in the previous considered cases.

Also, the obtained frequency values are comparable with those obtained by the other authors. If we look at the expression of the nondimensional time τ in the third of Equations (18), we notice that it would be the same as that utilized by the other above-mentioned authors, but for the presence of a coefficient π^2. This means that the time τ values should be divided by about 10, and the corresponding nondimensional

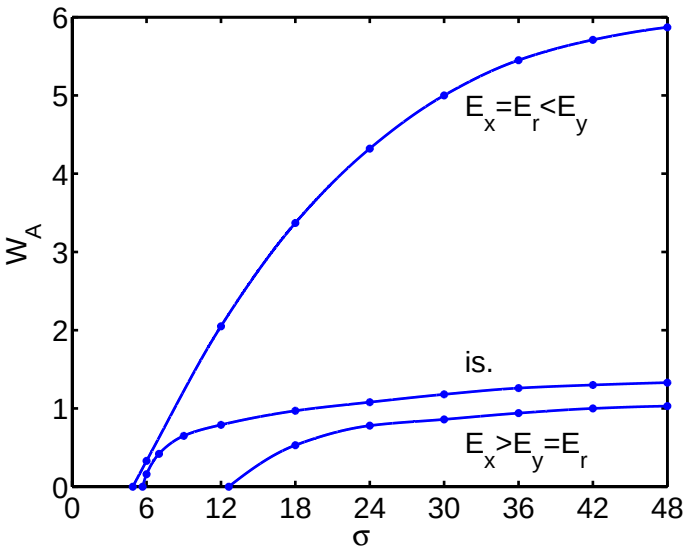

Figure 7. Behavior of the post-critical limit cycle amplitude W_A versus the nondimensional dynamic pressure λ in the sixth considered case.

λ	4.89	5.68	6.0	7.0	9.0	12.0	12.63	18.0	24.0	30.0	36.0	42.0	48.0
$E_x = E_r < E_y$	0.46		0.48			0.69		0.88	1.05	1.22	1.39	1.53	1.70
isotropic		0.70	0.72	0.9	1.3	1.85		2.95	4.0	4.76	5.85	6.75	7.48
$E_x > E_y = E_r$							3.3	4.9	6.35	7.70	9.01	10.31	11.40

Table 7. Values of the frequencies of the post-critical limit cycle versus the nondimensional dynamic pressure λ, in the sixth case.

Numerical parameters	Ritz	Ritz	Galerkin	Galerkin	FEM	FEM	FEM
N	30	42	36	64	80	120	168
W_A	5.838	5.872	5.856	5.872	5.941	5.903	5.881
ω	1.688	1.703	1.69	1.702	1.735	1.712	1.708
N	30	42	36	64	80	120	168
W_A	0.998	1.031	1.020	1.030	1.062	1.042	1.034
ω	11.383	11.402	11.398	11.401	11.443	11.421	11.410

Table 8. Values of amplitude and frequency in the sixth case for $\lambda = 48$, with $E_x = E_r < E_y$ (top) and $E_x > E_y = E_r$ (bottom), obtained by the three different methods with various values of the number N of the Lagrangian d.o.f.

frequency multiplied by the same coefficient for a significant comparison with the same parameter values obtained by the other authors. Thus it is reasonable to conclude that these derived frequency values are comparable with those shown in the graphs in [Ketter 1967; Eastep and McIntosh 1971].

Table 8 gives the values of the frequency and amplitude in the last case considered, corresponding to $\lambda = 48$ and for $(E_x > E_y = E_r)$ and $(E_x = E_r < E_y)$, and obtained by the three methods with different numbers of Lagrangian degrees of freedom. It is possible to evince the higher convergence rate of Ritz and Galerkin method with respect to the FEM, and the convergence of FEM results towards those of the two other methods, as the number of degrees of freedom grows indefinitely. It is evident enough that the amplitude values obtained by the three different methods are very close, and that the same chart lines would be derived by each method. The same is true for the previous cases considered, and the comparisons performed in this last case are sufficiently illustrative of the good agreement between the results obtained by the three different numerical schemes.

The meaning of the Table 9 is explained in the Appendix.

4. Discussion and conclusion

Concerning the post-critical flutter behavior of the vibrating panel, a significant effect of the plate elastic parameters on the amplitude of the limit cycle stationary solution has been detected. The importance of this amplitude value is fundamental, because, as mentioned earlier, it is a significant parameter of the vibrating panel resistance under the effects of a supersonic airflow.

$i_{\psi x}, i_{\psi y}$	$p_{i_{\psi x}}, p_{i_{\psi y}}$	N_d	N_p
1	4.712389	3.829886	
2	7.853982		17.923313
3	10.995574	86.324865	
4	14.137167		415.2424
5	17.278760	1997.5148	
6	20.420352		9608.99
7	23.561945	46223.87	
8	26.703538		222358.8966

Table 9. Values of $p_{i_{\psi x}}$, $p_{i_{\psi y}}$ and N_d, N_p versus $i_{\psi x}, i_{\psi y}$.

Furthermore, even a cursory examination of the obtained results is sufficient to conclude that the importance of the elastic Young's modulus in the flow direction is predominant with respect to the one in the perpendicular direction, as far as the flutter phenomenon is concerned.

In every case of the orthotropic fluttering plate if $E_x > E_y$, the amplitude of the post-critical limit cycle, is lower than the corresponding one with $E_x < E_y$. This fact is consistent with the results of [Shiau and Lu 1992], who found that the alignment of the fibers of a multilayer angle-ply laminate with the airflow direction diminishes the limit cycle amplitude, and consequently that the panel resistance to the flutter phenomenon grows. It is obvious that the smaller the angle between fibers and a reference axis in each lamina, the higher the Young's modulus of the equivalent orthotropic plate of the multilayer laminate along the same axis. Thus, with the increasing value of this modulus E_x along the flow direction, the vibration amplitude diminishes, and consequently it can be considered an elastic parameter of paramount importance as far as the limit cycle post-critical solution is concerned.

However the Poisson's moduli are also elastic parameters, which, after the above-mentioned one, play an important role in the considered phenomenon, because a remarkable effect of their values on the flutter amplitude can be evinced. (See Figures 3, 5 and 7.) In the corresponding cases considered, the Young's modulus of the isotropic reference plate is equal to the lower of the two Young's moduli of the orthotropic plate. The graphic curve of its flutter amplitude behavior versus λ lies between the two curves of the orthotropic plate. It means that the limit cycle amplitude of the isotropic plate is lower than the corresponding one of the orthotropic plate with $E_x = E_r < E_y$, although its Young's modulus E_r is equal to the smaller of E_x and E_y.

This fact bears further analysis. To this end it is necessary to recall the flexural rigidity moduli, introduced in Equation (3):

$$D_x = \frac{E_x h^3}{1 - \nu_{xy}\nu_{yx}}, \qquad D_y = \frac{E_y h^3}{1 - \nu_{xy}\nu_{yx}}. \tag{43}$$

It is evident that the Poisson's moduli ν_{xy}, ν_{yx} influence these out-of-plane rigidity parameters, because the higher their product is, the larger these parameters are. In these subcases with $E_x = E_r < E_y$ the Young's modulus E_r of the isotropic reference plate is equal to the lower one E_x of the orthotropic plate, but the Poisson's modulus $\nu_r = 0.3$ of the isotropic plate is larger than the two corresponding ones of the

orthotropic plate, as shown in Equations (41) and (42). Thus, although $E_r = E_x$, a value of this stiffness bending parameter $D_{x,is} = D_r$ along the x axis is obtained for the isotropic plate bigger than the one D_x of the orthotropic plate:

$$D_{x,is} = D_r = \frac{E_x h^3}{1-\nu_r^2} > D_x = \frac{E_x h^3}{1-\nu_{xy}\nu_{yx}}, \qquad 1-\nu_r^2 < 1-\nu_{xy}\nu_{yx}. \tag{44}$$

This means that there is a higher flexural rigidity along the airflow direction (coincident with the x axis direction) in the isotropic panel.

On the contrary, along the perpendicular y axis direction the Young's modulus E_y of the orthotropic plate is higher enough than E_r, so the flexural rigidity parameter D_y of the orthotropic plate is much larger than the corresponding one $D_{y,is} = D_r$ of the isotropic plate, in spite of the higher value of the Poisson's modulus ν_r with respect to both ν_{xy} and ν_{yx}:

$$D_{y,is} = D_{x,is} = D_r = \frac{E_r h^3}{1-\nu_r^2} < D_y = \frac{E_y h^3}{1-\nu_{xy}\nu_{yx}}, \qquad E_r = E_x \ll E_y. \tag{45}$$

Also, the modulus of mixed flexural rigidity between the two directions is important because, as in Equation (1), it influences the fluttering dynamics. This increases more than D_x when we pass from the orthotropic to the isotropic plate:

$$D_{xy,is} = \nu_r D_r = \nu_r \frac{E_r h^3}{1-\nu_r^2} > D_{xy} = \nu_{xy} D_y = \nu_{xy} \frac{E_y h^3}{1-\nu_{xy}\nu_{yx}}, \tag{46}$$

although, as above mentioned, E_y is much higher than $E_x = E_r$, but the product $\nu_r E_r$ is bigger than $\nu_{xy} E_y$ for both considered orthotropic panels, as seen from Equations (41) and (42). Furthermore this inequality is true also for the same other reason illustrated in Equation (44): $1-\nu_r^2 < 1-\nu_{xy}\nu_{yx}$.

Precisely the same holds for the extensional rigidity parameter $A_x = E_x h/(1-\nu_{xy}\nu_{yx})$ along the flow direction, which is smaller than the corresponding one $A_{x,is} = A_r = E_r h/(1-\nu_r^2)$ of the isotropic plate, although the Young's modulus E_r of the reference plate is equal to the lower of the two ones of the orthotropic plate, for the same reason stated earlier concerning the Poisson's moduli. A much higher value of $A_y = E_y h/(1-\nu_{xy}\nu_{yx})$ along the perpendicular direction corresponds to the orthotropic plate. The same thing is also true for the mixed extensional rigidity parameter, which is much higher for the isotropic plate.

The resulting effect is that the limit cycle amplitude is lower if the isotropic plate is employed with respect to the one of the orthotropic plate with fibers oriented in the perpendicular direction to the airflow, even if $E_r = E_x < E_y$, although the bending and extensional stiffness along the y axis direction of the orthotropic plate is much larger. In particular, increasing the flexural and extensional rigidity parameters in the airflow direction, along with the corresponding ones of the mixed rigidity, has an enhancing effect on the panel resistance to the flutter phenomenon much higher than increasing the same rigidity parameters in the perpendicular direction. This means that a much higher value of the Young's modulus of the orthotropic plate along the direction perpendicular to the airflow has lower influence on the considered phenomenon than a larger value of the Poisson's moduli—that is, the importance of these moduli ν_{xy}, ν_{yx} is predominant with respect to E_y.

If one looks carefully at Figures 3, 5 and 7, a further remark can be highlighted. For small values of the limit cycle amplitude, the $W_A - \lambda$ graphic curve of the isotropic plate is very near to the one of the orthotropic plate with $E_x = E_r < E_y$, but with the increasing dynamic pressure this curve tends to the one of the orthotropic plate with $E_x > E_y = E_r$, characterized by a higher resistance to the flutter phenomenon. This means that increasing the values of the Poisson's moduli correspondingly improves the resistance to the flutter phenomenon as the dynamic pressure grows.

Concerning the shear rigidity modulus $G_{xy} = G_{\Downarrow\hookleftarrow}$, no particular remarkable influence on the fluttering plate dynamics has been detected. In fact, in all the cases considered with $E_x = E_r < E_y$ this modulus is smaller for the isotropic plate. In the first considered orthotropic panel, whose elastic coefficients are defined in Equations (41), the value of this parameter of the reference isotropic plate is $G_{xy,is} = G_r = E_r/2(1+\nu_r) = 5.38\,\text{GPa}$, because $E_r = E_x = E_{\hookleftarrow} = 14\,\text{GPa}$, which is smaller than the corresponding one of the orthotropic plate $G_{\Downarrow\hookleftarrow} = 6$. But we have a much lower value of this parameter for the isotropic reference plate if the Young's modulus of the second considered orthotropic panel is assumed (see Equations (42)). In fact, $G_{xy,is} = G_r = E_r/2(1+\nu_r) = 2.69\,\text{GPa}$ because $E_r = E_x = E_{\hookleftarrow} = 7\,\text{GPa}$, and we have the same value of $G_{\Downarrow\hookleftarrow} = 6$. The resistance of the reference isotropic plate to the flutter phenomenon is higher than the one of both considered orthotropic panels, with the fibers aligned along the direction perpendicular to the airflow, even if $E_r = E_x < E_y$, for the above illustrated reason concerning the Poisson's moduli. Therefore decreasing the in-plane shear rigidity modulus has a quite negligible effect.

The use of three different numerical schemes to achieve the requested results, can offer a sufficient guarantee of the validity of the present numerical analysis, considering the good concordance between the results derived by the three methods. However, in some more complicated cases it could be difficult to apply the Galerkin method; in these more difficult circumstances, it would be useful to observe the slower convergence of the FEM results toward those of the Ritz procedure with the increasing number of d.o.f.; see [Tizzi 1994; 1999; 2003a].

Our analysis of flutter has been limited within the framework of the linearized piston theory. Yet it would seem relevant to know the influence of the nonlinear contribution to the aerodynamic forces on the permanent post-critical solution of the fluttering panel, confining attention to the limit cycle amplitude, which is particularly important for the reasons explained above. At a recent Italian congress (2005), we have presented evidence that also in post-critical conditions, if the dynamic pressure doesn't exceed overly much its critical value, limited effects of the nonlinear contributions to the aerodynamic forces can be seen. This would always be true but for the presence of particular initial conditions (such as those induced by a gust), which can instigate instability and chaos even before the critical value of the dynamic pressure is reached [Dessi et al. 2002]. Also, the presence of shock waves in transonic flight could instigate instability in the flutter phenomenon. It is indispensable to take into account the nonlinear contributions to aerodynamic forces in such cases, and this will undoubtedly be the focus of continued research.

Appendix

Functions utilized with Galerkin method in the free in-plane boundary conditions case. The functional elements of the nondimensional Airy function $\psi(\xi, \eta)$ series expansion in Equations (11) and (12), are

formed by two separate components, depending on ξ and η, respectively:

$$\varphi_{i_\psi}(\xi,\eta)=\varphi_{i_{\psi x}}(\xi)\varphi_{i_{\psi y}}(\eta),$$

where both components $\varphi_{i_{\psi x}}(\xi)$ and $\varphi_{i_{\psi y}}(\eta)$ vanish at the rectangular edges, along with their first normal derivatives:

$$\begin{aligned}
&\varphi_{i_{\psi x}}(0)=(\varphi_{i_{\psi x}})'(0)=\varphi_{i_{\psi x}}(1)=(\varphi_{i_{\psi x}})'(1)=0, \qquad (\,)'=\frac{\partial(\,)}{\partial\xi},\\
&\varphi_{i_{\psi y}}(0)=(\varphi_{i_{\psi y}})'(0)=\varphi_{i_{\psi y}}(1)=(\varphi_{i_{\psi y}})'(1)=0, \qquad (\,)'=\frac{\partial(\,)}{\partial\eta},
\end{aligned} \tag{A.1}$$

because, taking into account the membrane stresses dependence on the Airy function [Santini 1973], the in-plane boundary conditions in Equation (4) are satisfied. For convenience, functions are utilized which satisfy further conditions:

$$\frac{d^4\varphi_{i_{\psi x}}}{d\xi^4}=p_{i_{\psi x}}^4\varphi_{i_{\psi x}}, \qquad \frac{d^4\varphi_{i_{\psi y}}}{d\eta^4}=p_{i_{\psi y}}^4\varphi_{i_{\psi y}},$$

$$\int_0^1\varphi_{i_{\psi x}}\varphi_{j_{\psi x}}d\xi\cong\delta_{i_{\psi x}j_{\psi x}}, \qquad \int_0^1\varphi_{i_{\psi y}}\varphi_{j_{\psi y}}d\eta\cong\delta_{i_{\psi y}j_{\psi y}}.$$

Consequently the expressions of $\varphi_{i_{\psi x}}$ can be written as

$$\varphi_{i_{\psi x}}(\xi)=\frac{1}{N_d}\left\{\cos\Big(\frac{p_{i_{\psi x}}}{2}\Big)\cosh\Big[p_{i_{\psi x}}\big(\xi-\tfrac{1}{2}\big)\Big]-\cosh\Big(\frac{p_{i_{\psi x}}}{2}\Big)\cos\Big[p_{i_{\psi x}}\big(\xi-\tfrac{1}{2}\big)\Big]\right\},\quad i_{\psi x}=1,3,5,\ldots,$$

$$\varphi_{i_{\psi x}}(\xi)=\frac{1}{N_p}\left\{\sin\Big(\frac{p_{i_{\psi x}}}{2}\Big)\sinh\Big[p_{i_{\psi x}}\big(\xi-\tfrac{1}{2}\big)\Big]-\sinh\Big(\frac{p_{i_{\psi x}}}{2}\Big)\sin\Big[p_{i_{\psi x}}\big(\xi-\tfrac{1}{2}\big)\Big]\right\},\quad i_{\psi x}=2,4,6,\ldots,$$

where

$$p_{i_{\psi x}}=(2i_{\psi x}+1)\frac{\pi}{2}$$

and

$$N_d^2=\Big[\cosh\Big(\frac{p_{i_{\psi x}}}{2}\Big)\Big]^2\left[\frac{1}{2}-\frac{\cos\big(\frac{p_{i_{\psi x}}}{2}\big)\sin\big(\frac{p_{i_{\psi x}}}{2}\big)}{p_{i_{\psi x}}}\right]+\Big[\cos\Big(\frac{p_{i_{\psi x}}}{2}\Big)\Big]^2\left[\frac{1}{2}-\frac{\cosh\big(\frac{p_{i_{\psi x}}}{2}\big)\sinh\big(\frac{p_{i_{\psi x}}}{2}\big)}{p_{i_{\psi x}}}\right],$$

$$N_p^2=\Big[\sinh\Big(\frac{p_{i_{\psi x}}}{2}\Big)\Big]^2\left[\frac{1}{2}-\frac{\cos\big(\frac{p_{i_{\psi x}}}{2}\big)\sin\big(\frac{p_{i_{\psi x}}}{2}\big)}{p_{i_{\psi x}}}\right]+\Big[\sin\Big(\frac{p_{i_{\psi x}}}{2}\Big)\Big]^2\left[\frac{1}{2}-\frac{\cosh\big(\frac{p_{i_{\psi x}}}{2}\big)\sinh\big(\frac{p_{i_{\psi x}}}{2}\big)}{p_{i_{\psi x}}}\right],$$

and similarly for $\varphi_{i_{\psi y}}$, with $p_{i_{\psi y}}$ in place of $p_{i_{\psi x}}$ and η in place of ξ. The conditions in Equation (A.1) referring to the first derivatives are satisfied if it is taken into account that

$$\tan\Big(\frac{p_{i_{\psi x}},p_{i_{\psi y}}}{2}\Big)\cong 1$$

for the values of $p_{i_{\psi x}}$ and $p_{i_{\psi y}}$ used.

The values of $p_{i_{\psi x}}$, $p_{i_{\psi y}}$ connected with $i_{\psi x}$, $i_{\psi y}$, together with N_d, N_p, are summarized in Table 9, for $i_{\psi x}, i_{\psi y}=1,2,\ldots,8$.

References

[Abbas et al. 1993] J. F. Abbas, R. A. Ibrahim, and R. F. Gibson, "Nonlinear flutter of orthotropic composite panel under aerodynamic heating", *AIAA J.* **31**:8 (1993), 1478–1488.

[Bisplinghoff 1962] R. L. Bisplinghoff, *Principles of aeroelasticity*, Wiley, New York, 1962.

[Bolotin 1963] V. V. Bolotin, *Nonconservative problems of the theory of elastic stability*, MacMillan, New York, 1963.

[Crivelli Visconti 1975] I. Crivelli Visconti, *Materiali compositi – tecnologie e progettazione*, Tamburini, Milano, 1975.

[Dessi et al. 2002] D. Dessi, F. Mastroddi, and L. Morino, "Limit-cycle stability reversal near a Hopf bifurcation with aeroelastic applications", *J. Sound Vib.* **256**:2 (2002), 347–365.

[Dixon and Mei 1993] I. R. Dixon and C. Mei, "Finite element analysis of large-amplitude panel flutter of thin laminates", *AIAA J.* **31**:4 (1993), 701–707.

[Dowell 1966] E. H. Dowell, "Nonlinear oscillations of a fluttering plate", *AIAA J.* **4**:7 (1966), 1267–1275.

[Dowell 1967] E. H. Dowell, "Nonlinear oscillations of a fluttering plate, II", *AIAA J.* **5**:10 (1967), 1856–1862.

[Eastep and McIntosh 1971] F. E. Eastep and S. C. McIntosh, Jr., "Analysis of nonlinear panel flutter and response under random excitation or nonlinear aerodynamic loading", *AIAA J.* **9**:3 (1971), 411–418.

[Kantorowich and Krylov 1964] L. V. Kantorowich and V. I. Krylov, *Approximate methods of higher analysis*, Interscience, New York, 1964.

[Ketter 1967] D. J. Ketter, "Flutter of flat, rectangular, orthotropic panels", *AIAA J.* **5**:1 (1967), 116–124.

[Kikuchi 1986] N. Kikuchi, *Finite element methods in mechanics*, Cambridge University Press, Cambridge, 1986.

[Lambert 1991] J. D. Lambert, *Numerical methods for ordinary differential systems*, Wiley, Chichester, UK, 1991.

[Merson 1957] R. H. Merson, "An operational method for the study of integration processes", pp. 110–125 in *Proc. Symp. Data Processing* (Salisbury, S. Australia, 1957), Weapons Res. Establ. Salisbury, 1957.

[Mikhlin 1964] S. G. Mikhlin, *Variational methods in mathematical physics*, Pergamon Press, Oxford, 1964.

[Pars 1968] L. A. Pars, *A treatise on analytical dynamics*, Heinemann Educational Books, Ltd., London, 1968.

[Reddy 1986] J. N. Reddy, *Applied functional analysis and variational methods in engineering*, McGraw-Hill, New York, 1986.

[Reddy et al. 1988] J. N. Reddy, C. S. Krishnamoorthy, and K. N. Seetharamu, *Finite element analysis for engineering design*, Springer, Berlin, 1988.

[Santini 1973] P. Santini, *Introduzione alla teoria delle strutture*, Tamburini Editore, Milano, 1973.

[Shiau and Lu 1992] L. C. Shiau and L. T. Lu, "Nonlinear flutter of two-dimensional simply supported symmetric composite laminated plates", *J. Aircr.* **29**:1 (1992), 140–145.

[Tizzi 1994] S. Tizzi, "A numerical procedure for the analysis of a vibrating panel in critical flutter conditions", *Comput. Struct.* **50**:3 (1994), 299–316.

[Tizzi 1997] S. Tizzi, "Numerical procedure for the dynamic analysis of three-dimensional aeronautical structures", *J. Aircr.* **34**:1 (1997), 120–130.

[Tizzi 1999] S. Tizzi, "Free frequencies and modal shapes of cylindrical vibrating composite structures", *Comput. Struct.* **73**:6 (1999), 629–653.

[Tizzi 2003a] S. Tizzi, "Influence of non-linear forces on beam behaviour in flutter conditions", *J. Sound Vib.* **267**:2 (2003), 279–299.

[Tizzi 2003b] S. Tizzi, "Three numerical procedures for the post-critical flutter of an orthotropic plate", preprint, Aerospace and Astronautics Engineering Department, Università di Roma "La Sapienza", June 2003. Available at the web page for this paper.

[Xue and Mei 1993] D. Y. Xue and C. Mei, "Finite element nonlinear panel flutter with arbitrary temperatures in supersonic flow", *AIAA J.* **31**:1 (1993), 154–162.

[Zhou et al. 1994] R. C. Zhou, D. Y. Xue, and C. Mei, "Finite element time domain—modal formulation for nonlinear flutter of composite panels", *AIAA J.* **32**:10 (1994), 2044–2052.

[Zhou et al. 1995] R. C. Zhou, Z. Lai, D. Y. Xue, J. K. Huang, and C. Mei, "Suppression of nonlinear panel flutter with piezoelectric actuators using finite element method", *AIAA J.* **33**:6 (1995), 1098–1105.

[Zhou et al. 1996] R. C. Zhou, C. Mei, and J. K. Huang, "Suppression of nonlinear panel flutter at supersonic speeds and elevated temperatures", *AIAA J.* **34**:2 (1996), 347–354.

Received 9 Jul 2006. Revised 30 Nov 2006. Accepted 15 Feb 2007.

SILVANO TIZZI: s.tizzi@caspur.it
Aerospace and Astronautics Engineering Department, University of Rome "La Sapienza", Via Eudossiana 16, 00184 Rome, Italy